Correlation of spin and orbital anisotropies with chemical order in $Fe_{0.5}Pd_{0.5}$ alloy films using magnetic circular x-ray dichroism

P. Kamp,* A. Marty, B. Gilles, R. Hoffmann, S. Marchesini, and M. Belakhovsky
Département de la Recherche Fondamentale sur la Matière Condensée, SP2M CEA-Grenoble, France

C. Boeglin
IPCMS, Strasbourg, France

H. A. Dürr, S. S. Dhesi, and G. van der Laan
CCLRC Daresbury Laboratory, Warrington WA4 4AD, United Kingdom

A. Rogalev
ESRF, Grenoble, France

(Received 24 February 1998; revised manuscript received 28 July 1998)

The effects of chemical ordering in thin film $Fe_{0.5}Pd_{0.5}$ alloys, deposited by molecular-beam epitaxy directly on a MgO (001) substrate, have been studied using magnetic circular x-ray dichroism (MCXD) at the Pd and Fe $L_{2,3}$ edges. This system exhibits perpendicular magnetic anisotropy if grown in the $L1_0$ (001) phase and in-plane anisotropy in the disordered γ phase. We show that MCXD is a sensitive tool for studying variations in the spin and orbital magnetic moments due to changes in the chemical order. We obtain quantitative results for spin and orbital anisotropies and their variations with chemical order in the $Fe_{0.5}Pd_{0.5}$ alloy system. [S0163-1829(99)01602-1]

I. INTRODUCTION

Magnetic layers with a strong perpendicular magnetic anisotropy (PMA) are of great interest for magneto-optic recording media with predicted performances of up to 300 Gbit/inch^2, in comparison with present commercial hard disks which have storage densities around 2 Gbit/inch^2. Model systems are studied from a fundamental point of view, in order to get a better understanding of the microscopic magnetic properties and their relation with PMA. The quantitative determination of the magnetic moments and their anisotropies have been made possible by the application of sum rules to magnetic circular x-ray dichroism (MCXD) data, which allow us to derive element-specific orbital and spin magnetic moments. Furthermore, angle-dependent MCXD measurements lead to the orbital and spin anisotropies of the magnetic moments[1] that are directly related to the magnetocrystalline anisotropy energy (MAE). The orbital magnetic moment is influenced by the crystal field whereas the spin moment is only indirectly sensitive to it through the spin-orbit coupling.

PMA can be realized in several different ways, the principle being to overcome the demagnetizing energy by a perpendicular MAE. In the case of ultrathin surface layers[2,3] the PMA is due to the surface anisotropy while in multilayer systems such as Co/Au, Co/Pd, Co/Pt (Refs. 4–6) it is due to the interface anisotropy. For thicker layers, as in chemically ordered binary alloys, e.g., Refs. 7 and 8 on which the present study focuses, it is the bulk MAE that leads to PMA. These systems are particularly interesting for magneto-optic recording since, in addition to perpendicular anisotropy, the chemical ordering is accompanied by an increased Kerr rotation.[9]

A good candidate is the $Fe_{0.5}Pd_{0.5}$ system for which we were able to produce samples with PMA (Ref. 10) and have demonstrated the existence of perpendicular magnetic domains with a size of tens of nanometers.[11] This system offers the possibility of fabricating samples which possess either PMA or in-plane anisotropy while remaining in the same crystallographic structure, the fct lattice. This contrasts with other analogous systems like CoPt[7] where phase mixing occurs which complicates the study. By codeposition at 350 °C, the $L1_0$ tetragonal structure [CuAu(I)-type] is obtained, where the uniaxial chemical ordering leads to PMA.[10] We have also shown than PMA is preserved for less ordered cases, also obtained by molecular-beam-epitaxy (MBE) codeposition but at different temperatures. At room temperature the fully disordered γ phase is obtained, the magnetic moments are no longer perpendicular but in-plane, as sketched on the lower part of Fig. 1.

In this paper, we report on the study of the progression of the magnetic properties in a series of samples with varying chemical order and hence different MAE's. We show that the

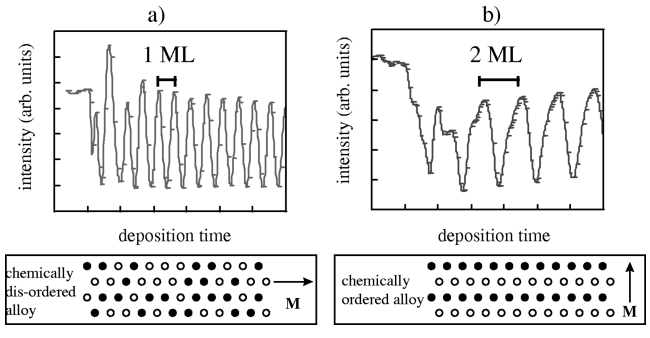

FIG. 1. RHEED control of the growth of a chemically disordered (a) and a chemically ordered sample (b). The γ and the $L1_0$ phases are sketched in (a) and (b), respectively.

TABLE I. Growth, structural, and magnetic data for the $Fe_{0.5}Pd_{0.5}$ films. The microscopic results are from MCXD spectroscopy on the Pd $L_{2,3}$ edges at sample orientation of 30°. $MAE_{rel}=1$ corresponds to 0.67 MJ/m^3.

$T_{deposition}$/°C ±10 °C	CO ±0.05	MAE_{rel} ±0.1	M_L/μ_B TEY ±0.005μ_B	M_S^{eff}/μ_B TEY ±0.03μ_B	M_L/μ_B FY ±0.005μ_B	M_S^{eff}/μ_B FY ±0.03μ_B
20	0.0	0	0.031	0.60	0.013	0.51
130	0.1	0.2	0.04	0.59		
lbl	0.3	0.82	0.043	0.58		
220	0.55	1	0.044	0.60	0.026	0.64
350	0.91	2.04	0.067	0.65	0.05	0.62
410	0.80	1.24	0.054	0.64		
510	0.66	1.95	0.049	0.61	0.025	0.68

MCXD spectroscopy at both the Pd and Fe $L_{2,3}$ edges is sensitive to the corresponding changes in effective spin and orbital magnetic moments. Quantitative results are obtained that can provide a further understanding on the microscopic origin of PMA and its relation to chemical ordering.

In Sec. II we describe the specimen used in the experiment and give in Sec. III the MCXD results obtained at the Pd $L_{2,3}$ and Fe $L_{2,3}$ edges. Section IV discusses the correlation between the magnetic moment anisotropies, the chemical order (CO), and the MAE.

II. EXPERIMENTAL

A. Sample preparation and characterization

Most of the alloy films were grown by codeposition of Fe and Pd directly onto MgO [001] substrates under UHV conditions, with typical growth rates around 0.5 Å /s.[8] The respective fluxes from the electron guns are controlled by two quartz balances, and calibrated before each deposition by reflection high-energy electron diffraction (RHEED). For the same flux of Fe and Pd atoms, we observe in Fig. 1 that the frequency of RHEED oscillations is doubled for an ordered sample with respect to a disordered one. This implies that the disordered alloy grows layer-by-layer, whereas the chemically ordered one grows bilayer by bilayer.

The samples under study here are 300 Å thick FePd films, deposited at substrate temperatures of 20, 130, 220, 350, 420, and 510 °C. One additional film was made by alternating deposition of Fe and Pd, atomic layer wise; we will refer to this sample as layer by layer or lbl. The 420 and the 510 °C samples show an increased roughness after deposition, respectively of 10 and 50 Å , compared to 3 Å for the other samples. This height modulation happens on a lateral scale of about 1 μm. An Al capping of 30 Å was deposited on top of each sample to prevent oxidation. The homogeneous growth of the FePd layers was checked by transmission electron microscopy (TEM) in sideview imaging. The onset of epitaxial growth occurs immediately at the MgO/FePd interface, with regular dislocations present in the first 30 Å to accommodate the 10% lattice mismatch.

The CO can be quantified by x-ray diffraction using $CO=|n_{Fe}-n_{Pd}|$, where n_{Fe} and n_{Pd} are the relative occupations of (e.g.) Fe atoms at the Fe and Pd lattice sites, following the procedure described in Ref. 10. We used the integrated intensities obtained from rocking scans for the [001]-[004] peaks. A completely disordered sample does not show the [001] and [003] superstructure peaks of the $L1_0$ phase. The best ordered samples are obtained at a growth temperature of 350 °C, and have an order parameter above $S=0.9$, i.e., 95% of the atoms are at their correct lattice site.

The FePd bulk alloy in the disordered γ phase (fcc) has a lattice parameter $a=3.8$ Å , while the MBE deposition leads to the fct tetragonalized phase, due to the strain induced by the larger MgO cubic substrate ($a=4.21$ Å). In our samples the tetragonalization increases slightly with the order parameter, as might be expected. For the 350 °C film, $a=3.89$ Å and $c=3.65$ Å , while the 20 °C film has $a=3.85$ Å and $c=3.76$ Å . The values of the samples grown at other temperatures reach values in between this range; for the lbl sample, $a=3.85$ Å and $c=3.72$ Å . The different tetragonalizations are correlated to the CO parameter and for the lbl and 130 °C samples we have deduced CO from the tetragonalization as the rocking curves of [001] and [003] become too small to be properly integrated.

Magnetic characterization was performed using vibrating-sample magnetometry and superconducting quantum interference device (SQUID) measurements.[11] The first technique is used to determine the hysteresis loops, from which the macroscopic MAE is deduced.[10] For perpendicular magnetic anisotropy the MAE is larger than the demagnetizing energy, which has a value of 0.67 ± 0.1 MJ/m^3 (Ref. 10) or 0.09 ± 0.014 meV/atom in $Fe_{0.5}Pd_{0.5}$. The ratios of the MAE to the demagnetizing energy, MAE_{rel} are collected in Table I, where one notices that the onset of a perpendicular easy axis takes place at $S=0.55$. The SQUID measurement was used to determine the saturation magnetization, which is 1150 ± 100 emu/cm^3 for all samples. This value corresponds to an average magnetic moment per atom of $1.46\pm0.15\mu_B$.

B. MCXD measurements

The MCXD spectra of the Pd $L_{2,3}$ edges, located at 3.333 and 3.173 keV, were measured on beamline ID12A of the European Synchrotron Radiation Facility (ESRF), Grenoble by fluorescence yield (FY) detection, and on station 3.4 of the Synchrotron Radiation Source (SRS), Daresbury by total electron yield (TEY). At the SRS, the sample normal was at

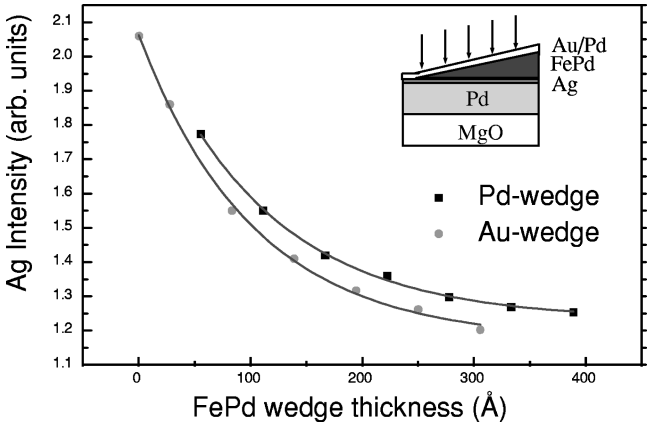

FIG. 2. Exponential attenuation of the signal from a buried Ag layer versus wedge thickness. The sample structure is shown in the inset, where arrows indicate the measured thicknesses.

30° and 55° relative to the x-ray beam direction. For the Ge(220) double-crystal monochromator used, the calculated degree of circular polarization on the sample is 74 and 48% at the Pd L_3 and L_2 edges, respectively. Both edges where recorded within the same scan, which was repeated after a 3 T field switching. At the ESRF, the FY was collected perpendicularly to the incident x rays in the horizontal plane, with the sample normal horizontal and at 30° and 60° from the beam. The beam characteristics were the same as in a previous Fe/Pd multilayer experiment;[12] the transmission through the Si(111) double-crystal monochromator reduces the 97% circular polarization rate from the HELIOS II undulator to 12.6 and 21.9% at the L_3 and L_2 edges, respectively. The samples were magnetized in a cryomagnet by a 3T field, large enough to saturate all samples in the geometries used. Spectra were recorded by scanning one edge for a given magnetic-field polarity, then switching it and scanning the same edge again. Reversing the helicity without changing the magnetic field resulted in similar signals, as expected. By measuring the Pd edges of the same samples both at the SRS and the ESRF, we found that the size of the polarization-corrected dichroic signals agreed within 1% . This suggests that the polarization rates given above are correct.

The FY probes equally the entire 300 Å thick films since the photon absorption length at the energy of the Pd edges is around 2 μm. Moreover, the self-absorption correction is small, with a maximum of 3% at the L_2 edge. In the case of TEY the probing depth has been studied, cf. Fig. 2, using two additional wedged samples whose structure is given in the inset. The attenuation depth have been found to be 108 ± 5 and 103 ± 7 Å for the Pd and Au-capped wedges, respectively.

In the Pd $L_{2,3}$ edges shown on Fig. 3, strong x-ray-absorption fine-structure (XAFS) oscillations are present beyond the white lines. These oscillations are a problem for the normalization, as they vary for samples with different degrees of chemical order. To reduce this problem we have taken long scans between the two edges and 200 eV above the L_2 edge. We smoothed the XAFS oscillations in these two regions with polynomials of second order and extrapolated them to the white lines. As a result we found the theoretical step ratio of 2:1 for the two edges within 2% for all

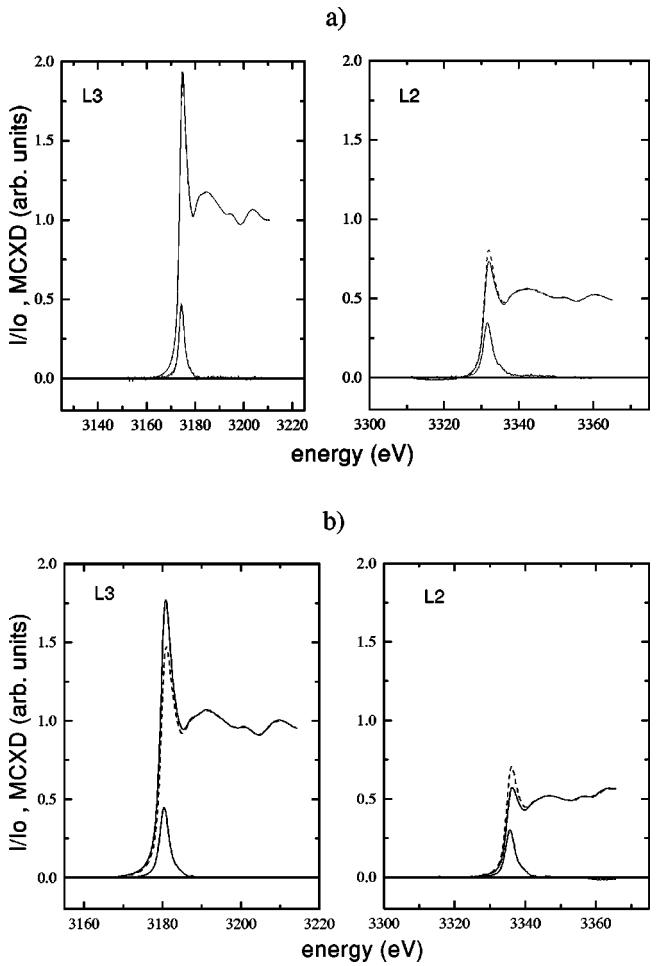

FIG. 3. Typical Pd $L2,3$ spectra taken by FY (a) and TEY (b). The XAS spectra are normalized, and the MCXD signals corrected for incomplete polarization. As evident on the XAS white line, the dichroic signal is very different in intensity between the two measurements, due mainly to the use of Si(111) and Ge(220) monochromators, respectively.

spectra. We used the same second-order polynomial fits to normalize the spectra prior to subtracting the spectra with opposite magnetic fields. The resulting dichroic signal was then corrected for the incomplete polarization of the x rays.

The MCXD measurements at the Fe $L_{2,3}$ edges were performed at SRS station 1.1, which is equipped with a spherical grating monochromator. The degree of polarization is 80% at both edges. The TEY detection used on the Fe $L_{2,3}$ edges corresponds to an escape depth around 20 Å , much lower than for the Pd $L_{2,3}$ edges. The Fe $L_{2,3}$ absorption spectra were all recorded in the geometry where the sample surface is perpendicular to the joint direction of the x-ray beam and the magnetic field. The treatment of the spectra and the background subtraction follows the procedures mentioned in the literature.[15]

III. MCXD RESULTS AND DISCUSSION

A. Data analysis and magnetic moments

Figure 3 shows typical normalized x-ray absorption spectroscopy (XAS) spectra at the Pd $L_{2,3}$ edges and the corresponding MCXD difference for a scan sequence of magnetic

field, obtained by FY and TEY. It is clear that the size of the dichroic effect differs between the two detection modes. This is due to the different degree of circular polarization. After correction for polarization, very similar MCXD spectra are obtained.

In order to separate the $2p \rightarrow 4d$ contributions in the white lines of the Pd L_3 and L_2 edges from other possible dipole transitions, we followed the method described in Ref. 12. Accordingly, we recorded the $L_{2,3}$ edges of a pure MBE-grown Ag thin film at both beam lines and normalized and scaled the Ag XAS spectra to the Pd edges. The integrated difference between the Pd and the Ag absorption spectra leads to the isotropic term $A3+A2$ in the expression of the sum rules given below. The numbers of holes were taken as $n_{4d}(\mathrm{Pd})=1.36$ (Ref. 13) and $n_{4d}(\mathrm{Ag})=0.35$. The same data treatment was used for all Pd $L_{2,3}$ spectra, enabling us to monitor accurately the changes in magnetic moments from sample to sample.

The spin and orbital moments were extracted using the sum rules[14]

$$\hat{\mathbf{P}}\cdot\mathbf{L}=-\frac{4}{3}\frac{\Delta A_3+\Delta A_2}{A_3+A_2}n_h; \tag{1a}$$

$$\hat{\mathbf{P}}\cdot\mathbf{S}^{\mathrm{eff}}\equiv\hat{\mathbf{P}}\cdot\mathbf{S}+\frac{7}{2}\hat{\mathbf{P}}\cdot\mathbf{T}=-\frac{\Delta A_3-2\Delta A_2}{A_3+A_2}n_h, \tag{1b}$$

where $\Delta A_{2,3}$ are the integrated intensities over the MCXD signals at the $L_{2,3}$ edges, n_h the difference between the number of Pd and Ag d holes, and $\mathbf{T}$ is the expectation value of the magnetic dipole term. Along the x-ray direction defined by the unit vector $\hat{P}$, we will refer to the projections of the orbital magnetic moment as M_L and to that of the effective spin magnetic moment as $M_{\mathrm{eff}}^S=M_S-7M_T$.

The general trend of the dichroic results, which will be put on a quantitative basis in Sec. III B, can already be appreciated from Figs. 4(a)–4(c). The first two figures show the MCXD signals of the Pd $L_{2,3}$ edges from different samples in the 30° geometry, taken in the TEY mode. A regular evolution of the dichroic peak height is seen on the zoomed spectra for both edges, as the MBE deposition temperature increases from 20 to 350 °C, i.e., as the degree of CO increases. In addition, one can notice that the variation of the dichroic signal for the Pd L_2 edge behaves differently from that of the L_3—the maximum change being 11 instead of 20%—indicating that the orbital moment is affected by the chemical order.

As an example, in Fig. 4(c) a comparison is presented for the Pd L_2 edge recorded by FY, between the 30° and 60° orientations. In contrast to the large intensity variation observed at 30°, the MCXD spectra taken at 60° exhibit similar peak heights. We infer from these raw data that the spin and orbital magnetic moments measured in the latter geometry do not show a significant variation with CO. Moreover the 60° signals are located within the margins given by the ones at 30°. This indicates a sign change in the magnetic anisotropies with chemical order.

Quantitatively, the application of the sum rules leads to the magnetic moments compiled in Table I. Comparing the orbital moments obtained for Pd from TEY and FY, we find the latter to be systematically slightly smaller. There may be

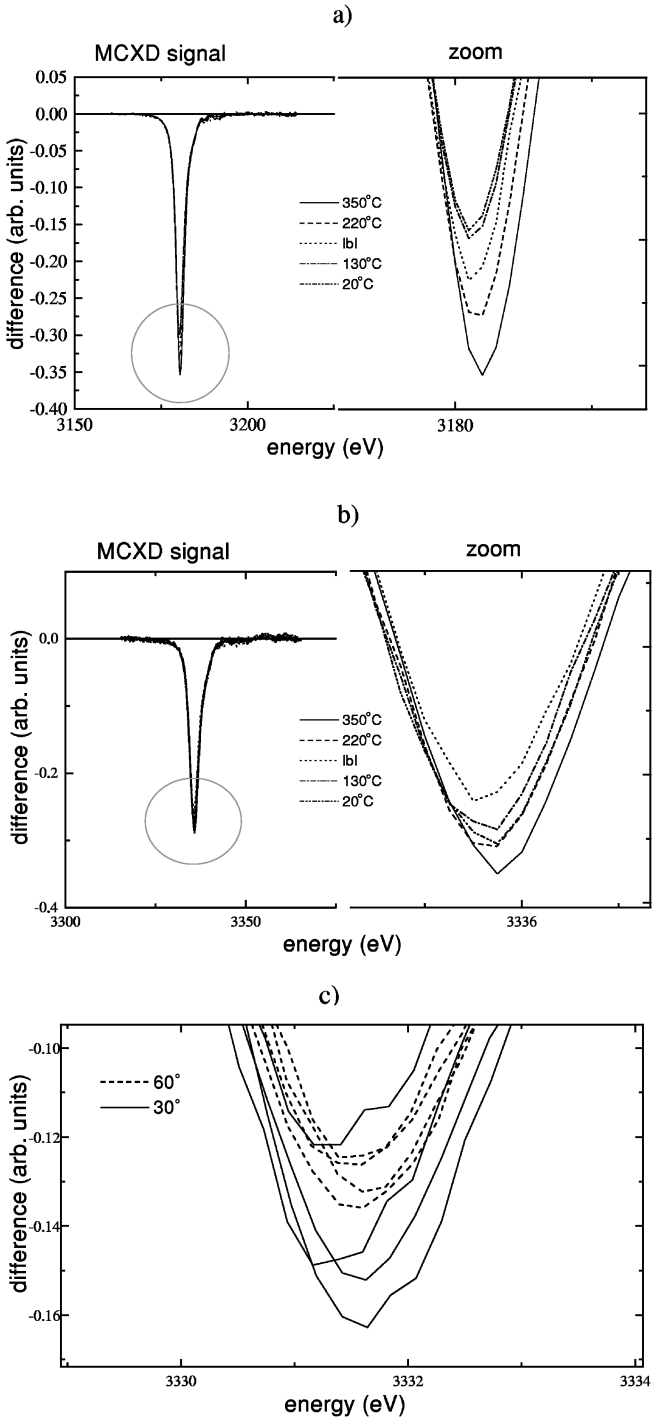

FIG. 4. Pd L_3 edges (a) and Pd L_2 edges (b) as measured at 30° with TEY detection. The enlarged peaks show a regular evolution with chemical order; on (c), the Pd L_2 edge is given for two sample orientations, 30°, continuous, and 60°, dashed line, in the case of FY mode. The 60° data is confined in range, in contrast with the 30° one (cf. text).

several reasons for this difference. First, the fluorescence signal is not strictly proportional to the absorption coefficient, however, the Pd L edges are a favorable case.[12] In addition our samples are thin compared to the photon attenuation length; whereas the TEY is more sensitive to the upper part of the film. Second, the experimental resolutions and the degree of polarization are different and may lead to slight

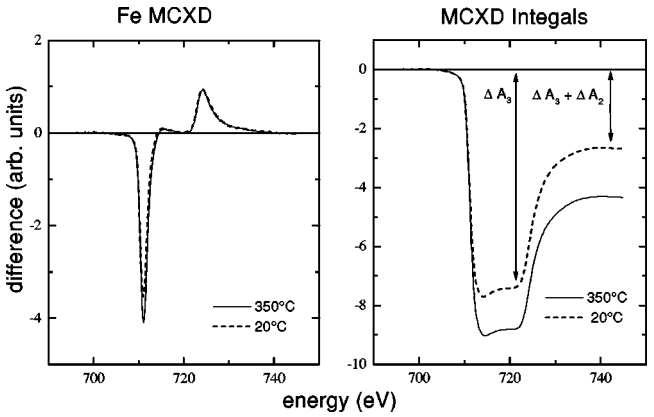

FIG. 5. Fe $L_{2,3}$ dichroism and the corresponding sum rule integrals. The sample normal was parallel to the x-ray beam.

differences. Third, the information in fluorescence and total yield measurements are averaged over different sample areas. With FY the Al/FePd and FePd/MgO interfaces contribute to the signal. In particular, the interface FePd/MgO is characterized by a 30 Å area with structural defects (dislocations in the FePd lattice).

One might question the accuracy of the absolute values of the magnetic moments. The application of the sum rules requires knowledge of the number of d holes in the valence band, which is obtained from band-structure calculation. Furthermore, separating the contributions of $4d$, $5s$, and continuum transitions by applying the Ag background subtraction method leads to some uncertainty. To have an idea of the absolute accuracy, we compared the average moment by SQUID measurements, $1.46\pm0.15\mu_B$ with the total Fe bulk moment, taken from Ref. 15 and the total Pd moment measured with fluorescence detection which gives $1.45\pm0.10\mu_B$. Since both techniques are averaging over the whole FePd layer, we believe that the absolute values are correct within 10%.

However, far more important in our analysis are the variations between the samples, which are directly obtained from the integration over the MCXD curves. Recalling the reproducibility of the XAS background between the spectra of opposite magnetic field selected in our data treatment, cf. Fig. 4, we estimate the relative error to be significantly smaller than the absolute one, as the smooth variation with the CO will confirm below. In Table I, we present for the different MBE conditions the orbital and spin magnetic moments deduced from the measurements performed in the two detection modes in the 30° geometry, together with the CO parameter and the relative $\mathrm{MAE_{rel}}$. Correlations between CO, $\mathrm{MAE_{rel}}$, M_L, and M_s are immediately noticeable.

Effective spin and orbital moments measured at 60° are, as anticipated, nearly constant for the different samples. The averaged experimental values obtained with FY are: $M_s^{\mathrm{eff}}=0.58\pm0.03\mu_B$ and $M_L=0.038\pm0.005\mu_B$. In the TEY detection mode the values collected at 55° are: $M_s^{\mathrm{eff}}=0.62\pm0.03\mu_B$ and $M_L=0.046\pm0.005\mu_B$.

We now turn to the Fe case. The MCXD spectra on the Fe $L_{2,3}$ edges are shown in Fig. 5 for the two extreme cases, 20 and 350 °C, respectively, corresponding to the chemical disordered and best ordered FePd alloys. These Fe spectra are obtained with perpendicular orientation of the sample (0°). They show a large change with CO and the integrated intensities, using the sum rules, also evidence this difference of both spin and orbital moments. The effective spin and orbital moments for Fe are $M_s^{\mathrm{eff}}=2.04\pm0.05\mu_B$ and $M_L=0.42\pm0.05\mu_B$ in the chemically ordered sample and $M_s^{\mathrm{eff}}=2.13\pm0.05\mu_B$ and $M_L=0.22\pm0.05\mu_B$ in the disordered one. Compared to bulk bcc Fe, where MCXD measurements give an orbital moment of $0.09\,\mu_B$,[15] M_L is twice as large in the 20 °C sample and four times larger in the ordered 350 °C one. The spin moment M_s^{eff} is less affected by the chemical order of the alloy, the changes being within the error bars. The orbital and spin values are close to those reported by Le Cann *et al.*[2] for ultrathin Fe/Pd (100) films, where interdiffusion favors interface alloying.

B. Correlation with chemical order and MAE

1. Pd magnetic moments and CO parameters

We will mainly base the discussion on the TEY results, for which a complete set of data is available and therefore the evolution from sample to sample can be followed with a high degree of accuracy. However, for some important parameters, a comparison with the FY data will be made. The variation of the CO parameter with the MBE deposition temperature is simple to interpret. The order increases with temperature up to a maximum value of CO=0.91 at 350 °C. Then, since the deposition temperatures are getting too close to the order/disorder transition temperature, the CO starts to decrease. The effective spin moment M_s^{eff} and orbital moment M_L, deduced from the MCXD data at 30°, are represented as a function of CO in Figs. 6(a) and 6(b). The smooth variation of these moments, both fitted with a third-order polynomial, gives further evidence of the small relative uncertainty in the treated data. The effective spin moment goes through a minimum corresponding to the lbl sample at CO=0.3, whereas a monotonic variation of much larger amplitude is observed for the orbital moment. Both quantities reach their maximum for the most ordered sample. The M_L value is more than doubled between the 20 and 350 °C samples. Another consequence of these variations relates to the discussion about the relevant range of chemical order which affects the magnetic properties. It is interesting to observe that the dichroic data correlates clearly with the CO.

2. Pd spin and orbital anisotropies

Since the TEY measurement at 55° is close to the magic angle of 54.7° where the spin sum rule gives the pure spin moment instead of the effective moment,[16] the experimental result shows that M_s is independent of the chemical order, i.e., it is not sensitive to the variation of the crystalline field around the Pd atom. Its value is $M_s=0.62\,\mu_B$ within 3%. The insensitivity of M_s to variations of the local arrangement could be expected, since it is quadratic in the ξ/E_{ex} ratio, where ξ is the spin-orbit coupling parameter and E_{ex} is the exchange energy for the Pd $4d$-derived bands. This is not the case for the orbital moment, which is linear in this ratio.[14] The variation of the effective spin moment at 30° (cf. Table I) is therefore characteristic of a sizable spin-dipole term. Up to now, such a term has been neglected by most authors. Here we have clear experimental evidence of its contribution

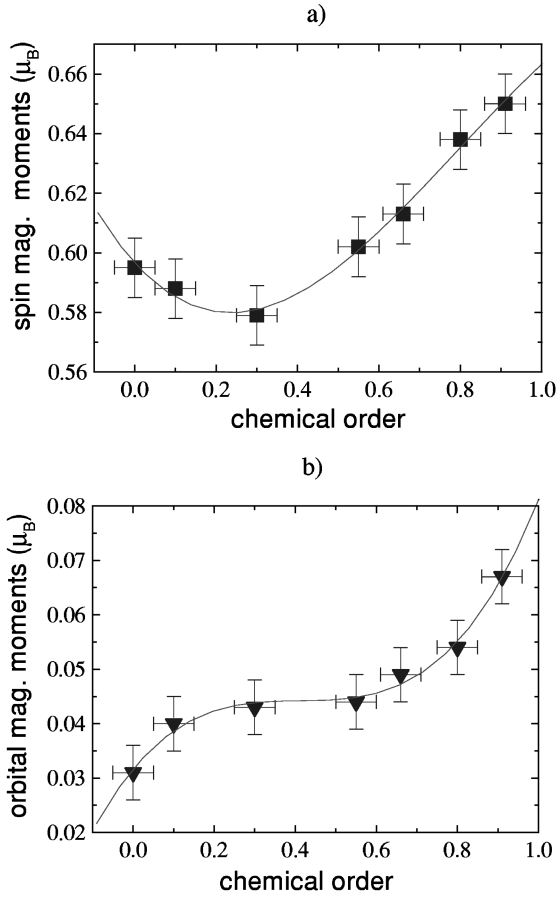

FIG. 6. The spin (a) and orbital (b) Pd magnetic moments are given versus the CO parameter. The continuous line is a third-order polynomial fit.

to the spin sum rule. The same conclusion can be drawn using the fluorescence data. For the most ordered case, we use the method of Ref. 16 to obtain the M_T component parallel to the surface $7M_T^{\parallel}=0.032$ and $0.024\,\mu_B$, leading to a large spin dipole anisotropy: $7M_T^{\perp}-7M_T^{\parallel}=-0.04$ or $-0.06\,\mu_B$, in the FY and TEY modes, respectively. A similar argument applies to the orbital moment. At the magic angle, only the isotropic part of the orbital moment will be observed,[17] and indeed we obtained a value independent from the local environment: $M_L^{\rm iso}=0.046$ or $0.038\,\mu_B$, in the electron and fluorescence modes, respectively. The variation of the orbital moment at 30° is clearly apparent from Table I, with the largest value corresponding to the best ordered sample. From the angular data, we deduce the parallel and perpendicular components of the orbital moment in this uniaxial case by: $M_L(\gamma)=M_L^{\parallel}\cdot\sin^2\gamma+M_L^{\perp}\cdot\cos^2\gamma$ and $3M_L^{\rm iso}=M_L^{\perp}+2M_L^{\parallel}$, where $\gamma=30°$ is the joint direction of x rays, magnetic field, and M_s. For the ordered case, the resulting orbital moment is $M_L^{\parallel}=0.028\,\mu_B$ from both measurements. The orbital anisotropy is $M_L^{\perp}-M_L^{\parallel}=+0.05$ or $+0.03\,\mu_B$, from TEY and FY modes, respectively. Repeating the same procedure for all samples measured in the electron detection mode, it is straightforward to deduce the spin and orbital anisotropies between the perpendicular and in-plane directions. Their variations, represented in Figs. 7(a) and 7(b), follow naturally those of the effective spin and orbital moments of Fig. 6. One remarkable feature is that both anisotropies go from negative to positive when the CO increases. The orbital anisotropy vanishes near the switching from a parallel to a perpendicular easy axis of magnetization (cf. Table I, $\mathrm{MAE_{rel}}=1$).

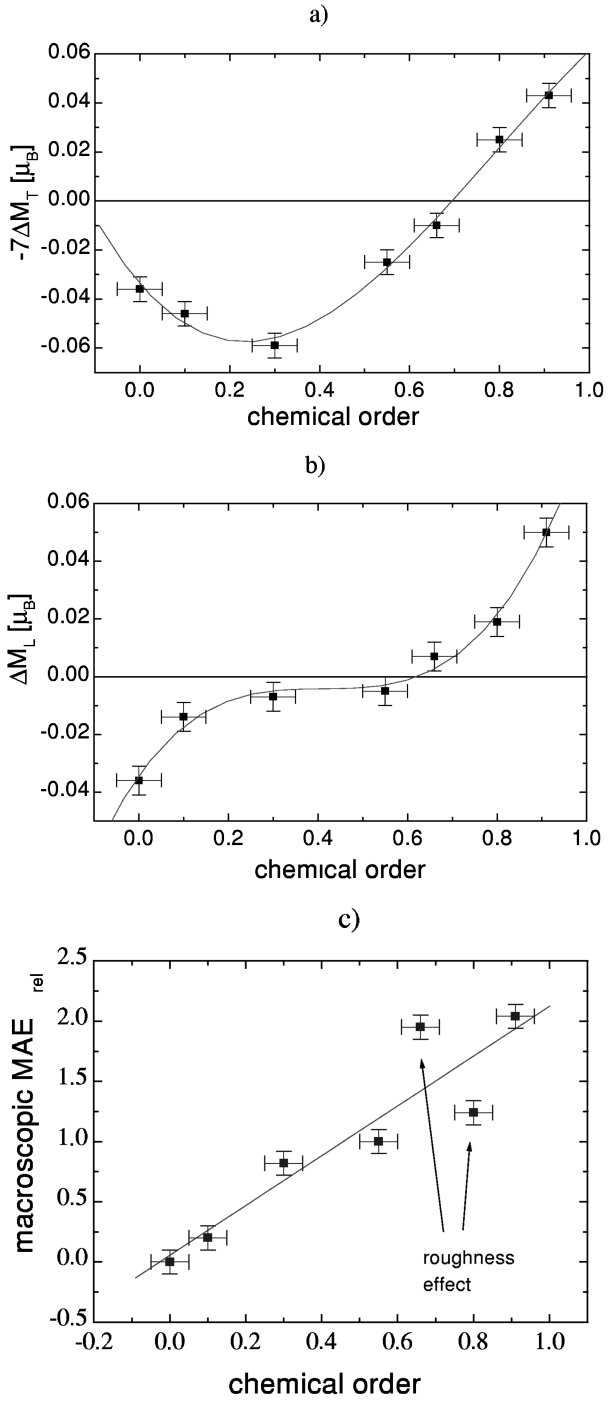

FIG. 7. Evolution of spin (a) and orbital (b) anisotropies of the Pd magnetic moments in TEY mode with CO. The global macroscopic MAE is given in (c).

3. Macroscopic and microscopic MAE

The macroscopically determined MAE increases rather linearly with the CO, as seen in Fig. 7(c). It is zero for the disordered 20 °C sample and reaches a relative value of 2.0 at 350 °C. There is, however, some scatter for the 420 and

510 °C samples. This can be ascribed to the fact that the model used to determine the MAE assumes the samples to be thin flat layers, whereas in reality they present a high degree of roughness at elevated deposition temperatures.

In the limit that the ground-state spin-orbit coupling ξ is small compared to the crystal field and to the exchange interaction E_{ex}, one can express the microscopic MAE according to Ref. 18 as

$$\mathrm{MAE} = -\frac{\xi}{4\mu_B}[(M_L^{\perp}-M_L^{\parallel})^{\uparrow}-(M_L^{\perp}-M_L^{\parallel})^{\downarrow}] + \frac{3\xi^2}{2\mu_B E_{ex}}(7M_T^{\perp}-7M_T^{\parallel}). \quad (2)$$

For a quantitative prediction of the first term one needs to know the difference between the Pd spin ↑ and ↓ *d* states, whereas only the sum can be obtained from the MCXD measurements. If we neglect the spin ↓ part, the first term would lead to a too large value of 1.7 meV per Pd atom in the ordered case. We recall that the macroscopic magnetic result is 0.18 meV per atom. Concerning the second term, the condition $E_{ex} \gg \xi$ breaks down since, for the Pd $4d$-derived bands in FePd, both $\xi = E_{ex} = 0.17$ eV. Indeed, the second term would give much too high a contribution (around 15 meV per Pd atom), using our result for the magnetic dipole anisotropy. However, we will assume in the following that a more realistic second term is still linear in the spin anisotropy $7MT^{\perp}-7MT^{\parallel}$. It is clear from Figs. 7(b) and 7(c) that the orbital anisotropy decreases the MAE. In the case of the magnetic dipole anisotropy, the MAE first increases for the less ordered samples; then from $S=0.3$, its contribution adds to the orbital part to decrease the MAE. More quantitative predictions on the microscopic understanding of the Pd contribution to MAE will await *ab initio* calculations and the experimental results presented here provide a stringent test for such calculations.

Looking to the Fe moments in the 20 and 350 °C samples, we observe a variation of M_L and M_s^{eff} different from those of the Pd moments. The effective spin moment decreases from $2.13\mu_B$ (20 °C) to $2.04\mu_B$ (350 °C), while the orbital moment increases from $0.22\mu_B$ (20 °C) to $0.42\mu_B$ (350 °C). These values bear similarities with those measured by Le Cann *et al.*[2] The spin moments are smaller than those from pure Fe, $M_s^{\mathrm{eff}} = 2.19\mu_B$, while the orbital moments are strongly enhanced compared to pure Fe, $M_L = 0.09\,\mu_B$. The SQUID measurements on FePd, that do not see the spin and orbital anisotropic components, give an average magnetic moment per atom of $1.46\,\mu_B$. The average of the total Pd moment measured in FePd at 60° with fluorescence detection and of the total Fe moment from pure Fe is $1.45\mu_B$. Lacking angular Fe data, we suggest the Fe moments measured in FePd at 55° to be the same as the bulk ones. Under this assumption, we find an MAE of 0.24 meV/atom for Fe. This value is only slightly larger than the average, macroscopically determined MAE, which would suggest that the Pd atoms make an important contribution to the overall MAE.

IV. CONCLUSION

We have shown that in FePd binary alloys which exhibit PMA, the MAE and the magnetic moments are strongly correlated to the CO. The FePd system is an ideal model for such a study as the local magnetic anisotropy effects on both Pd and Fe are large, while the crystallographic structure is simple and does not change with the CO.

We have used MCXD to determine the Fe and Pd spin and orbital moments, as well as their evolution as a function of CO, with a high degree of accuracy. Macroscopic techniques such as SQUID were unable to detect this evolution. The induced Pd moments are quite large, similar to pure Ni, and the Fe orbital moments are strongly enhanced, reaching values close to those of surface layers.

By using the angular dependence of MCXD we have determined unambiguously the orbital and spin dipole anisotropies, which vary smoothly with the CO, as characterized by x-ray diffraction. These anisotropies are key parameters in the microscopic and element-specific MAE, and both contribute to favor the PMA at large CO. A more complete understanding of the MAE will require a strong interplay between our results and *ab initio* band-structure calculations.

Our approach, using the MCXD technique, can be used as a relatively simple method to determine whether PMA can be achieved by alloy ordering or by multilayered structures.

The FePd system is a well suited candidate for the transverse MCXD geometry,[17] since the variations of orbital and spin anisotropies could be measured with even higher accuracy and give additional information on their orientation for both elements.

ACKNOWLEDGMENTS

P.K. and S.M. acknowledge the European Union for grants under Contracts No. ERBFMBICT950524 and No. ERBFMBICT961366. We thank J.A.D. Matthew for providing access to the MCXD facility at Daresbury under Grants No. EPSRC J82195 and No. L68568. The MCXD experiments at ESRF, Grenoble, were done under Ref. HE-219. We thank A. Smith for help during the SRS measurements and H. Ebert for the calculation of the *d* holes.

*Also at Heinrich Heine Universität Düsseldorf, Germany.

[1] J. Stöhr and H. König, Phys. Rev. Lett. **75**, 3748 (1995).
[2] X. Le Cann, C. Boeglin, B. Carrière, and K. Hricovini, Phys. Rev. B **54**, 373 (1996).
[3] H. A. Dürr, G. van der Laan, J. Lee, G. Lauhoff, and J. A. C. Bland, Science **277**, 213 (1997).
[4] W. B. Zeper, F. J. A. M. Greidanus, P. F. Garcia, and C. R. Finscher, J. Appl. Phys. **65**, 4971 (1989).
[5] C. H. Lee, R. F. C. Farrow, C. J. Lin, E. E. Marinero, and C. J. Chien, Phys. Rev. B **42**, 11 384 (1990).
[6] T. Sugimoto, T. Katayama, Y. Suzuki, M. Hashimoto, Y. Nishihara, A. Itoh, and K. Kawanishi, J. Magn. Magn. Mater. **104-107**, 1845 (1992).
[7] M. Maret, M. C. Cadeville, R. Poinsot, A. Herr, and E. Beaurepaire, J. Magn. Magn. Mater. **166**, 45 (1997).
[8] R. F. C. Farrow, D. Weller, R. F. Marks, and M. F. Toney, J. Appl. Phys. **79**, 5967 (1996).
[9] V. Gehanno, Ph.D. thesis, INPG, Grenoble, 1997.

[10] V. Gehanno, A. Marty, B. Gilles, and Y. Samson, Phys. Rev. B **55**, 12 552 (1997).
[11] V. Gehanno, Y. Samson, A. Marty, B. Gilles, and A. Chamberod, J. Magn. Magn. Mater. **172**, 26 (1997).
[12] J. Vogel, A. Fontaine, V. Cros, F. Petroff, J. P. Kappler, G. Krill, A. Rogalev, and J. Goulon, Phys. Rev. B **55**, 3663 (1997).
[13] H. Ebert (private communication).
[14] B. T. Thole, P. Carra, F. Sette, and G. Van der Laan, Phys. Rev. Lett. **68**, 1943 (1992); P. Carra, B. T. Thole, M. Altarelli, and X. Wang, *ibid.* **70**, 694 (1993); G. van der Laan, Phys. Rev. B **57**, 112 (1998).
[15] C. T. Chen, Y. U. Idzerda, H.-J. Lin, N. V. Smith, G. Meigs, E. Chaban, G. H. Ho, E. Pellegrin, and F. Sette, Phys. Rev. Lett. **75**, 152 (1995).
[16] D. Weller, J. Stöhr, R. Nakajima, A. Carl, M. G. Samant, C. Chappert, R. Mégy, P. Beauvillain, P. Veillet, and G. A. Held, Phys. Rev. Lett. **75**, 3752 (1995).
[17] H. A. Dürr and G. van der Laan, Phys. Rev. B **54**, R760 (1996).
[18] G. van der Laan, J. Phys.: Condens. Matter **10**, 3239 (1998).